Available online at www.sciencedirect.com
ScienceDirect
Trans. Nonferrous Met. Soc. China 32(2022) 1513−1529
Transactions of Nonferrous Metals Society of China
www.tnmsc.cn

Characterization of hot deformation and microstructure evolution of a new metastable β titanium alloy

Zhao-qi CHEN[1,2], Li-juan XU[1,2], Shou-zhen CAO[3], Jian-kai YANG[1,2], Yun-fei ZHENG[1,2], Shu-long XIAO[1,2], Jing TIAN[1,2], Yu-yong CHEN[1,2]

1. National Key Laboratory for Precision Hot Processing of Metals, Harbin Institute of Technology, Harbin 150001, China;
2. School of Materials Science and Engineering, Harbin Institute of Technology, Harbin 150001, China;
3. College of Mechanical and Electrical Engineering, Huangshan University, Huangshan 245021, China

Received 12 April 2021; accepted 29 October 2021

Abstract: The hot deformation characteristics of as-forged Ti−3.5Al−5Mo−6V−3Cr−2Sn−0.5Fe−0.1B−0.1C alloy within a temperature range from 750 to 910 ℃ and a strain rate range from 0.001 to 1 s^{-1} were investigated by hot compression tests. The stress−strain curves show that the flow stress decreases with the increase of temperature and the decrease of strain rate. The microstructure is sensitive to deformation parameters. The dynamic recrystallization (DRX) grains appear while the temperature reaches 790 ℃ at a constant strain rate of 0.001 s^{-1} and strain rate is not higher than 0.1 s^{-1} at a constant temperature of 910 ℃. The work-hardening rate θ is calculated and it is found that DRX prefers to happen at high temperature and low strain rate. The constitutive equation and processing map were obtained. The average activation energy of the alloy is 242.78 kJ/mol and there are few unstable regions on the processing map, which indicates excellent hot workability. At the strain rate of 0.1 s^{-1}, the stress−strain curves show an abnormal shape where there are two stress peaks simultaneously. This can be attributed to the alternation of hardening effect, which results from the continuous dynamic recrystallization (CDRX) and the rotation of DRX grains, and dynamic softening mechanism.

Key words: metastable β titanium alloy; hot deformation behavior; microstructure evolution; abnormal flow behavior

1 Introduction

Since its first successful application in aerospace in the 1950s, titanium alloys have received extensive attention and rapid development due to their unique properties. Among them, the metastable β high-strength titanium alloys have become important aerospace materials in recent decades due to their excellent properties such as good welding performance, good hardenability, and good heat treatment performance [1,2]. Therefore, the metastable titanium alloys are mainly used to replace high-strength structural steel components on aircraft, which can reduce aircraft weight by 30%−40% [3,4].

The metastable β titanium alloys are often used in aircraft landing gears, fuselages, wings and other load-bearing or stressed parts [5], which means that the alloy needs to have good workability and microstructure. Thermomechanical processing (TMP) is one of the most important processing methods for the manufacture of titanium alloy parts [6,7]. It can achieve the adjustment of microstructure during the forming process, so that the parts can obtain excellent mechanical properties. Besides, the performance of the alloy is significantly affected by thermal deformation,

Corresponding author: Li-juan XU, E-mail: xljuan@hit.edu.cn; Shu-long XIAO, E-mail: xiaoshulong@hit.edu.cn
DOI: 10.1016/S1003-6326(22)65890-4

which depends on deformation parameters and initial structure [8]. During TMP, dynamic recovery (DRV) and dynamic recrystallization (DRX) occur inside the material, which directly affect the structure and properties. Therefore, it is very important to study the flow behavior of the alloy under different parameters, e.g. different temperatures and strain rates, during hot deformation. GAO et al [9] recently summarized the experimental characterization and modeling of the hot deformation behavior and microstructure evolution of titanium alloys. The common dynamic softening occurring during hot deformation was attributed to many aspects, including deformation heating, the occurrence of DRV and DRX, the spheroidization of lamellar α, and elaborated the influence mechanism of each aspect on the flow behavior. In addition, constitutive analysis and hot processing map are important tools to study the hot deformation behavior [10−12]. RAVINDRANATH and VEMURI [13] conducted compression tests on the Ti-5553 alloy at different temperatures and strain rates and established the constitutive equation. WANG et al [14] preformed hot compression experiments on the TB7 alloy under different conditions, studied the DRV and DRX processes during the hot deformation and established the hot working map.

The Ti−3.5Al−5Mo−6V−3Cr−2Sn−0.5Fe−0.1B−0.1C is a new type of metastable β titanium alloy. The addition of B and C was to form the TiB and TiC reinforcements, which can improve performance to a large extent, and has been studied in many works [15,16]. The previous research of our group [17] has carried out solution and aging treatment on the alloy and found that the strength of the alloy can reach 1637 MPa with an acceptable elongation of 5.6%, which shows that this alloy has great potential for application in the aerospace field. However, the hot deformation behavior of the Ti−3.5Al−5Mo−6V−3Cr−2Sn−0.5Fe−0.1B−0.1C alloy has less been studied yet. The present work conducted uniaxial hot compression tests on Ti−3.5Al−5Mo−6V−3Cr−2Sn−0.5Fe−0.1B−0.1C alloy under different conditions. The evolution of the microstructure and flow behavior during the hot deformation were analyzed with the establishment of constitutive equations and processing map to provide guidance for the hot working process of the alloy.

2 Experimental

The starting material was prepared by vacuum induction melting technology. The ingot was cleaned and the surface defects were removed to prevent cracking during the forging process. Subsequently, the ingot was forged in multiple passes at 980, 870 and 790 °C as a final forging to modify the as-cast microstructure. The as-forged microstructure indicated a typical bimodal feature, which has been studied in previous research [17]. The β transus temperature was approximately (815±5) °C, which was measured by the metallographic method.

The hot compression tests were conducted on a Gleeble−1500 thermo-mechanical simulator using cylindrical specimens with 8 mm in diameter and 12 mm in height, which were machined from the as-forged material. To reduce friction, graphite sheets were placed on both ends of the specimens. The tests were carried out at temperatures from 750 to 910 °C with an interval of 40 °C and strain rates of 0.001, 0.01, 0.1 and 1 s^{-1}. The height reduction was set to be 60% and the heating rate was 10 °C/s. To ensure homogeneous temperature fields, the specimens were heated to the desired temperature and held for 2 min before the tests. After the tests, each specimen was water-quenched immediately to retain the deformed microstructure for subsequent analysis.

Microstructure observation was performed on an optical microscope (OM) and a scanning electron microscope (SEM). The specimens were first ground with SiC abrasive papers from 400 to 2000 grits. To meet the surface requirements, the specimens were electropolished at 35 V for 90 s using a solution of 60% methanol, 30% *n*-butanol alcohol and 10% perchloric acid. For OM observations, the specimens were then etched in the Kroll's reagent (10 mL HF, 30 mL HNO_3 and 200 mL H_2O). EBSD analysis was conducted on ZEISS SUPRA55 field emission scanning electron microscope with an EBSD detector and the Channel 5 software.

3 Results and discussion

3.1 Flow behavior

Figure 1 shows the true stress−strain curves of

the Ti−3.5Al−5Mo−6V−3Cr−2Sn−0.5Fe−0.1B−0.1C alloy obtained in the hot deformation tests to height reductions of 60%. It can be found that when the strain exceeds 0.6, the stress value shows an obvious upward trend, which is different from the typical stress−strain curves. Although in the present work graphite flakes are added to the two ends of the sample to reduce friction during the experiment, it still cannot avoid the friction between the alloy and the indenter when the amount of deformation is large. This unexpected part of the experimental data does not affect the experimental results, so it is not shown in Fig. 1. It can be found that as the temperature increases and the strain rate decreases, the flow stress gradually decreases. As the strain increases, almost all curves except the ones at the strain rate of 0.1 s^{-1} show similar trends that the flow stress first increases to a peak value, then gradually decreases and finally stabilizes. After the peak (σ_p), the stress−strain curves show obvious dynamic softening characteristics, which can be mainly attributed to dynamic recovery (DRV) and dynamic recrystallization (DRX) [18]. Besides, it was also found that deformation heating [19], dynamic spheroidization of α phase [20] and loss of Hall−Petch strengthening [21] may also cause softening behaviors. In the initial stage of deformation, the critical stress of deformation requires the increment of dislocations [22] and the dislocation density inside the alloy increases rapidly. These dislocations entangle with each other and hinder the movement of subsequent dislocations, which is manifested as the increase in flow stress and called the work-hardening effect. After the peak value, as shown in Fig. 1, at relatively low strain rates (0.001, 0.01 and 0.1 s^{-1}), the stress−strain curve of the alloy shows typical DRX characteristics that the stress is significantly reduced. When the strain rate is increased to 1 s^{-1}, the stress almost maintains a constant value, indicating the occurrence of DRV.

Furthermore, as the temperature increases and the strain rate decreases, the average kinetic energy of atoms is increased and the movement of dislocations is enhanced. Figure 2 shows the trend of peak stress during hot deformation. Similar trends are also found in other literatures [10,23]. CHEN et al [24] reported that DRX is more likely

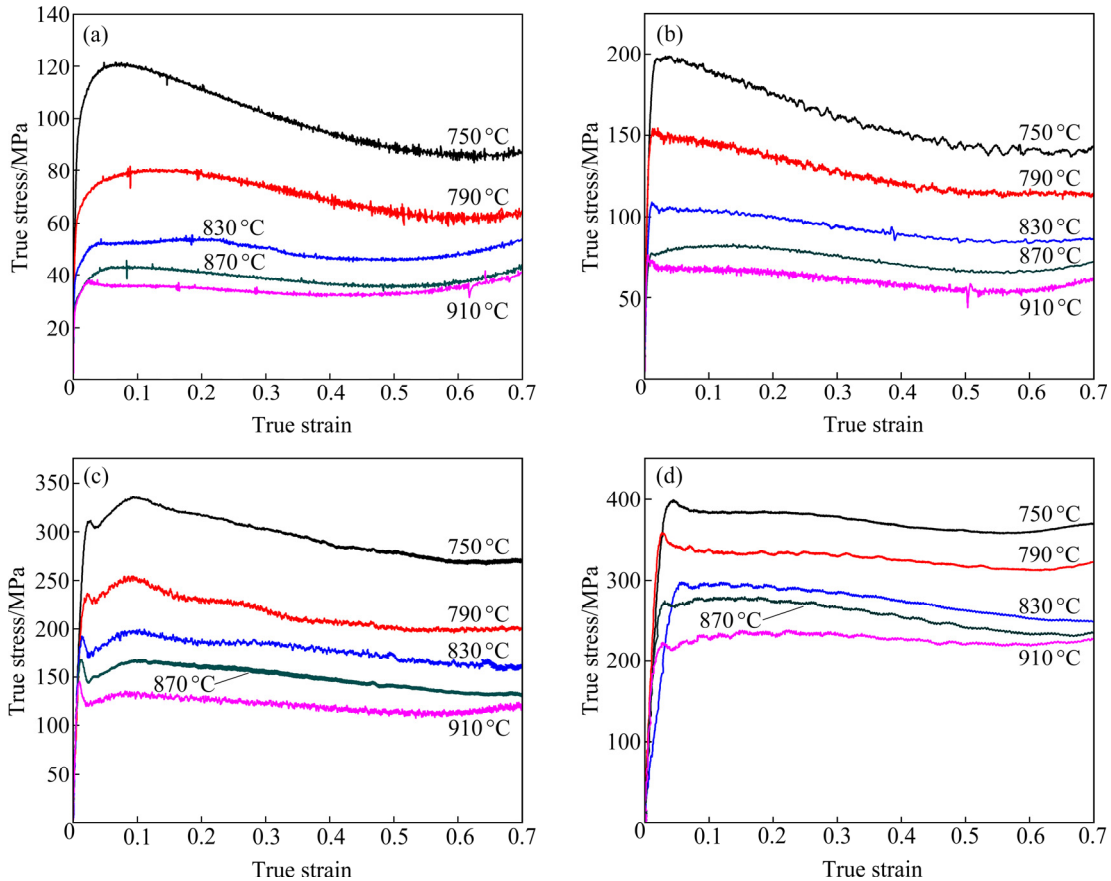

Fig. 1 Stress−strain curves during hot compression of Ti−3.5Al−5Mo−6V−3Cr−2Sn−0.5Fe−0.1B−0.1C alloy at different strain rates: (a) 0.001 s^{-1}; (b) 0.01 s^{-1}; (c) 0.1 s^{-1}; (d) 1 s^{-1}

to occur under conditions of high deformation temperature and low strain rate, which is ascribed to the good mobility of dislocations at high temperatures and sufficient diffusion time at low strain rates. Both occurrences of DRV and DRX greatly reduce the dislocation density and lead to the reduction of flow stress. Thus, the DRV and DRX behavior can result in the reduction of flow stress, especially at high temperatures and low strain rates. Besides, the β transus temperature of the alloy has been measured to be 815 °C, so the phase transformation that occurs during the hot deformation of the alloy also affects the flow stress of the alloy. When the deformation temperature is lower than 815 °C, the alloy is composed of α phase (hcp structure) and β phase (bcc structure), which determines that α phase has less effective slip systems than β phase. As the deformation temperature increases, the volume fraction of α phase in the alloy gradually decreases, which reduces the critical shear stress for deformation of the alloy. Therefore, the peak stress shows a tendency to decrease with the increase of temperature.

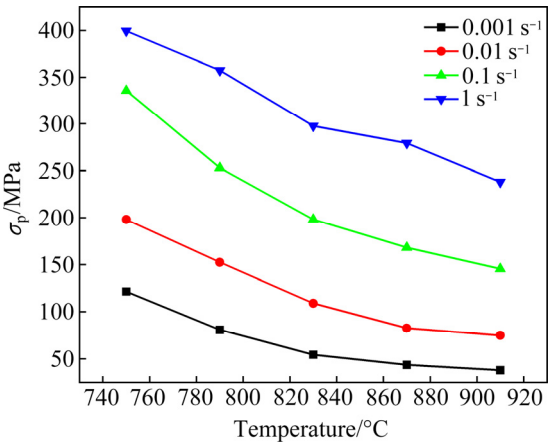

Fig. 2 Peak flow stress of Ti−3.5Al−5Mo−6V−3Cr−2Sn−0.5Fe−0.1B−0.1C alloy deformed under different conditions

3.2 Microstructure evolution

Figure 3 shows the microstructure of Ti−3.5Al−5Mo−6V−3Cr−2Sn−0.5Fe−0.1B−0.1C alloy undergoing hot deformation experiments at different temperatures and a constant strain rate of 0.001 s^{-1}. When the deformation temperature is 750 °C, it can be found that the grains in the structure have undergone significant elongation perpendicular to the compression direction and no recrystallized grains can be found. In addition, since the deformation temperature is lower than the β transus temperature of the alloy at this time, there are two phases with different contrasts in the structure, namely α and β arrowed in Fig. 3(a). When the temperature rises to 790 °C, it is difficult to distinguish the contrast of the two phases even though the temperature is still lower than the β transus temperature at this time. This phenomenon can be attributed to the low free energy difference and the large cooling rate. The former makes the $\beta\rightarrow\alpha$ transformation kinetics small, while the latter makes the $\beta\rightarrow\alpha$ transformation time insufficient, which is also found in Ref. [25]. Compared with the grains of the alloy deformed at 750 °C, the elongation of the grains is obviously weakened. In addition, zigzag grain boundary provides sites for grain nucleation, so it can be found that fine recrystallized grains are formed at the grain boundary. As the temperature further increases, the microstructure presents a completely normalized contrast at 830 °C, indicating that the alloy is composed of β-single phase at this time. Some recrystallized grains grow up and some new fine recrystallized grains are formed at the triple junction of the adjacent grain boundaries. The number of sub-grain boundaries increases significantly, and the grain boundaries of the initial grains become equiaxed. As shown in Fig. 3(d), a large number of sub-crystalline structures are generated inside the β grains and the grains are separated by these sub-structures to appear in the form of multiple adjacent equiaxed grains. When the temperature is contained to increase to 910 °C, the alloy structure is mainly composed of coarsened equiaxed grains. A large number of subcrystalline structures and recrystallized grains can be clearly found, which indicates that the recrystallization process of the alloy proceeds sufficiently at this time.

Figure 4 shows the microstructure of Ti−3.5Al−5Mo−6V−3Cr−2Sn−0.5Fe−0.1B−0.1C alloy undergoing hot deformation experiments at different strain rates and a constant temperature of 910 °C. It can be found that as the strain rate increases, the degree of deformation of the alloy increases significantly. As shown in Fig. 4(d), when the strain rate is 1 s^{-1}, it can be found that the β grains in the alloy have obvious elongation along the direction perpendicular to the compression direction. When the strain rate decreases to 0.1 s^{-1}, recrystallized grains begin to appear and the volume

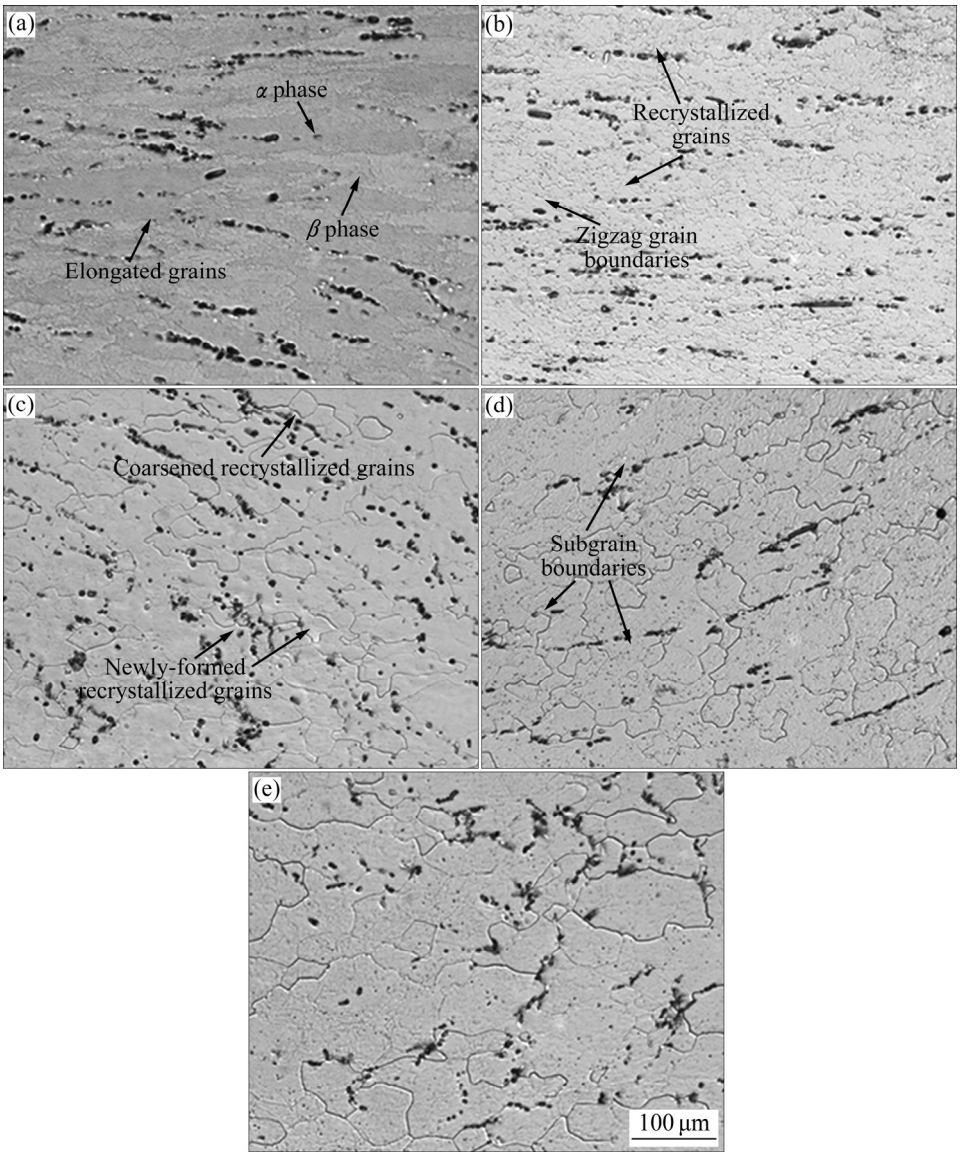

Fig. 3 Micrographs of Ti−3.5Al−5Mo−6V−3Cr−2Sn−0.5Fe−0.1B−0.1C alloy after thermal compression at strain rate of 0.001 s^{-1} and different deformation temperatures: (a) 750 °C; (b) 790 °C; (c) 830 °C; (d) 870 °C; (e) 910 °C

fraction increases with the decrease of the strain rates. At the strain rate of 0.001 s^{-1}, almost all the grains are equiaxed, indicating that DRX is easier to occur under the condition of the low strain rate.

To further study the microstructure evolution and mechanical properties, the EBSD analysis was carried out on the Ti−3.5Al−5Mo−6V−3Cr−2Sn−0.5Fe−0.1B−0.1C alloy deformed at 910 °C and 0.001 s^{-1}, as shown in Fig. 5. Figure 5(b) shows the grain boundary map of the alloy, in which the low-angle grain boundaries (LAGBs, 2°−15°) are represented by red lines, and the high-angle grain boundaries (HAGBs, >15°) are represented by blue lines. The recrystallized grains are mainly formed by HAGBs, which is consistent with the results of other literatures [18,26]. The appearance of a large number of sub-crystalline structures inside the grains indicates that the alloy has undergone a rearrangement of dislocations during the deformation process. As the strain increases, not only a large number of dislocations are generated inside the grains, but also stress concentration is formed at the grain boundaries. To reduce the stress concentration, the dislocations inside the grains are rearranged, which presents the LAGBs [27]. As the deformation process continues, the LAGBs gradually transform into HAGBs with the rotation of grains. In this process, the dislocation density inside the grains drops significantly, which leads to a change in the flow stress of the alloy.

Figure 5(c) shows the grain orientation map of the alloy after hot deformation, in which the

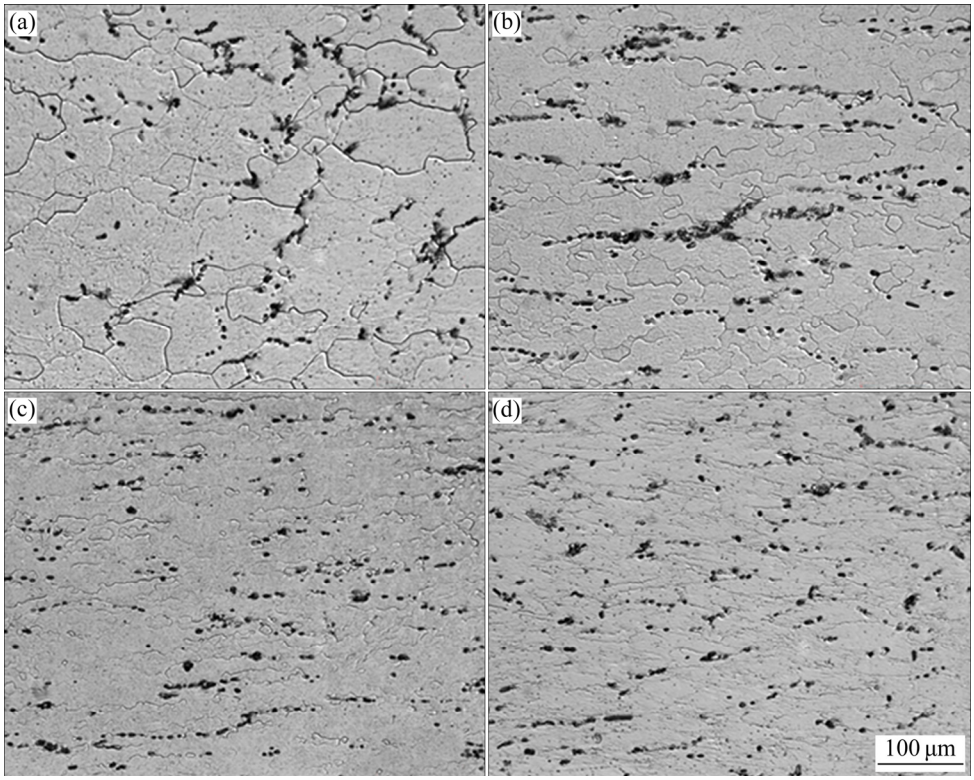

Fig. 4 Micrographs of Ti−3.5Al−5Mo−6V−3Cr−2Sn−0.5Fe−0.1B−0.1C alloy after thermal compression at 910 °C and different strain rates: (a) 0.001 s^{-1}; (b) 0.01 s^{-1}; (c) 0.1 s^{-1}; (d) 1 s^{-1}

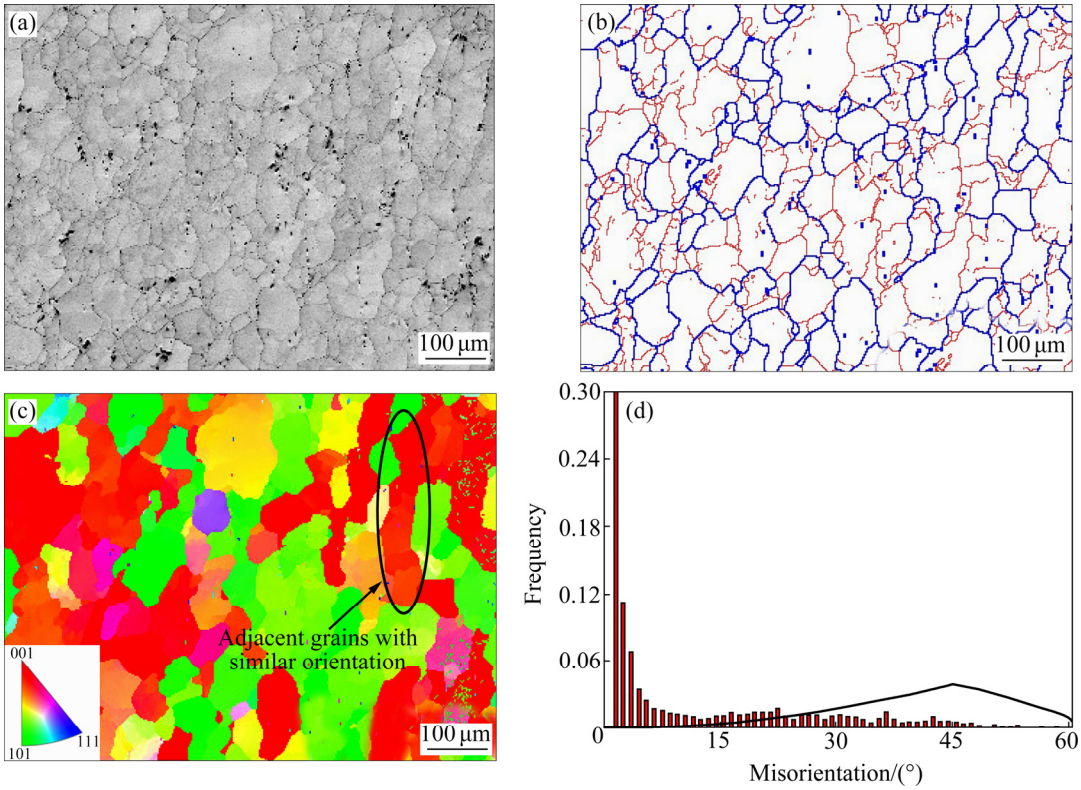

Fig. 5 EBSD analysis results of alloy deformed at 910 °C and 0.001 s^{-1}: (a) Microstructure; (b) Grain boundary map; (c) Grain orientation map; (d) Misorientation angle distributions

orientation gradient of the crystal grains is represented by the color gradient and can be obtained by the key stereographic triangle. It can be found that the grains in the microstructure mainly show a strong orientation of ⟨100⟩, which is in line with the research results of REID and OWEN [28].

Moreover, from the position indicated by the arrow in Fig. 5(c), it can be found that the orientations of several adjacent grains are basically the same, which means that these grains may be the same grain before deformation, and gradually separate during the deformation process. Misorientation angle distribution is shown in Fig. 5(d). Most of the grain boundaries are still LAGBs, but the HAGBs also account for a relatively high proportion of about 32.9%. The HAGBs are mainly formed by DRX [18,29], which shows that after hot deformation under this condition, the recrystallization of the alloy has reached a high degree of completion. The curve in Fig. 5(d) represents the random orientation distribution of grains. It can be found that there is a large difference between the actual orientation and the random orientation, indicating that there is a phenomenon of preferential orientation in the alloy. Figure 6 shows the pole figures and inverse pole figures of the alloy and a strong {100}⟨100⟩ texture is found.

3.3 Work hardening behavior

In addition to temperature, the strain rate is also an important parameter that affects the microstructure evolution of the alloy. It can be seen from Fig. 4 that as the strain rate decreases, the characteristics of DRX become more dominant, which is related to the occurrence of work-hardening effect [30]. In the present study, to investigate the work hardening behavior, we use two different methods to obtain the work hardening curves.

(1) For most deformation cases, firstly, the compression curves shown in Fig. 1 are fitted by nonlinear fitting method with fitting equation of $\sigma=[A_1+A_2\ln\varepsilon+A_3(\ln\varepsilon)^2+A_4(\ln\varepsilon)^3+A_5(\ln\varepsilon)^4]/[B+A_6\ln\varepsilon+A_7(\ln\varepsilon)^2+A_8(\ln\varepsilon)^3+A_9(\ln\varepsilon)^4]$, in which A_1, A_2, A_3, A_4, A_5, A_6, A_7, A_8, A_9 and B are unknown parameters. Then, taking derivative of the fitting curves can obtain the required work-hardening curves.

(2) For some special deformation parameters, the fitting equation used is not accurate enough to substitute compression curves. Thus, we choose to smooth the curves by filtering every three data points and then take derivative.

Figure 7 shows all the work hardening curves of the Ti−3.5Al−5Mo−6V−3Cr−2Sn−0.5Fe−0.1B−0.1C alloy. The following points can be found: (1) As the deformation continues, the work hardening rate θ of the alloy gradually decreases, which is consistent with the dynamic softening mechanism produced by DRV and DRX. (2) When the deformation temperature remains unchanged, as the strain rate decreases, θ decreases significantly.

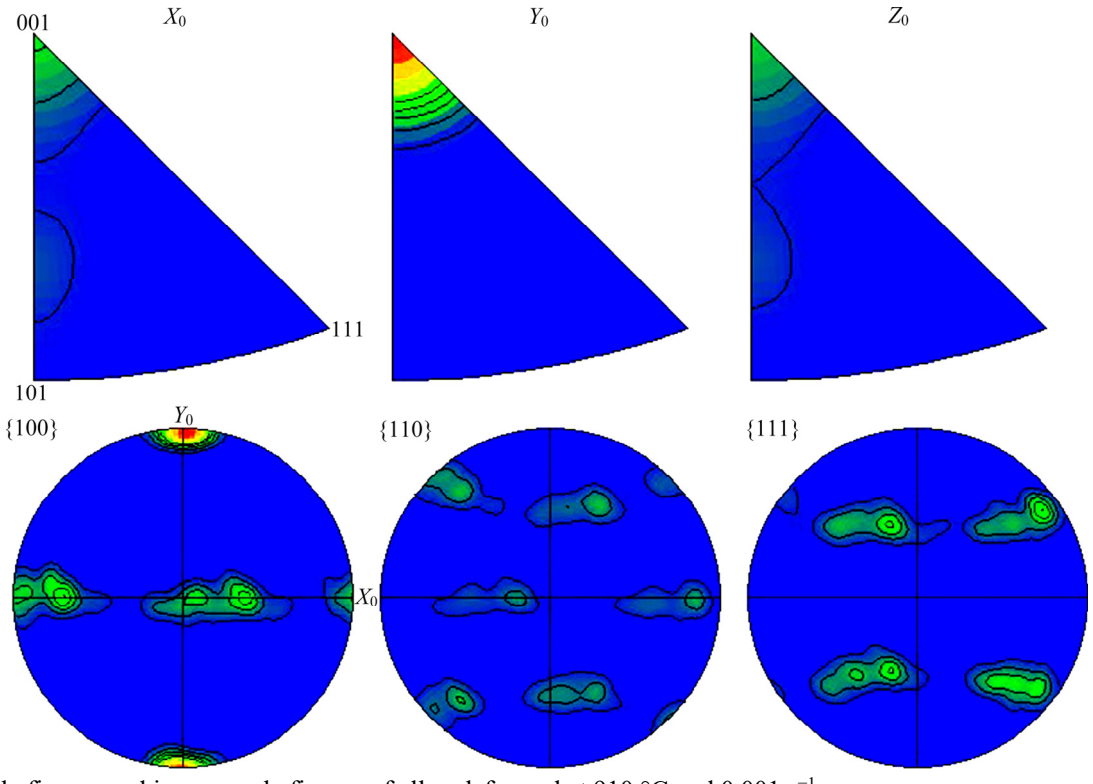

Fig. 6 Pole figures and inverse pole figures of alloy deformed at 910 °C and 0.001 s^{-1}

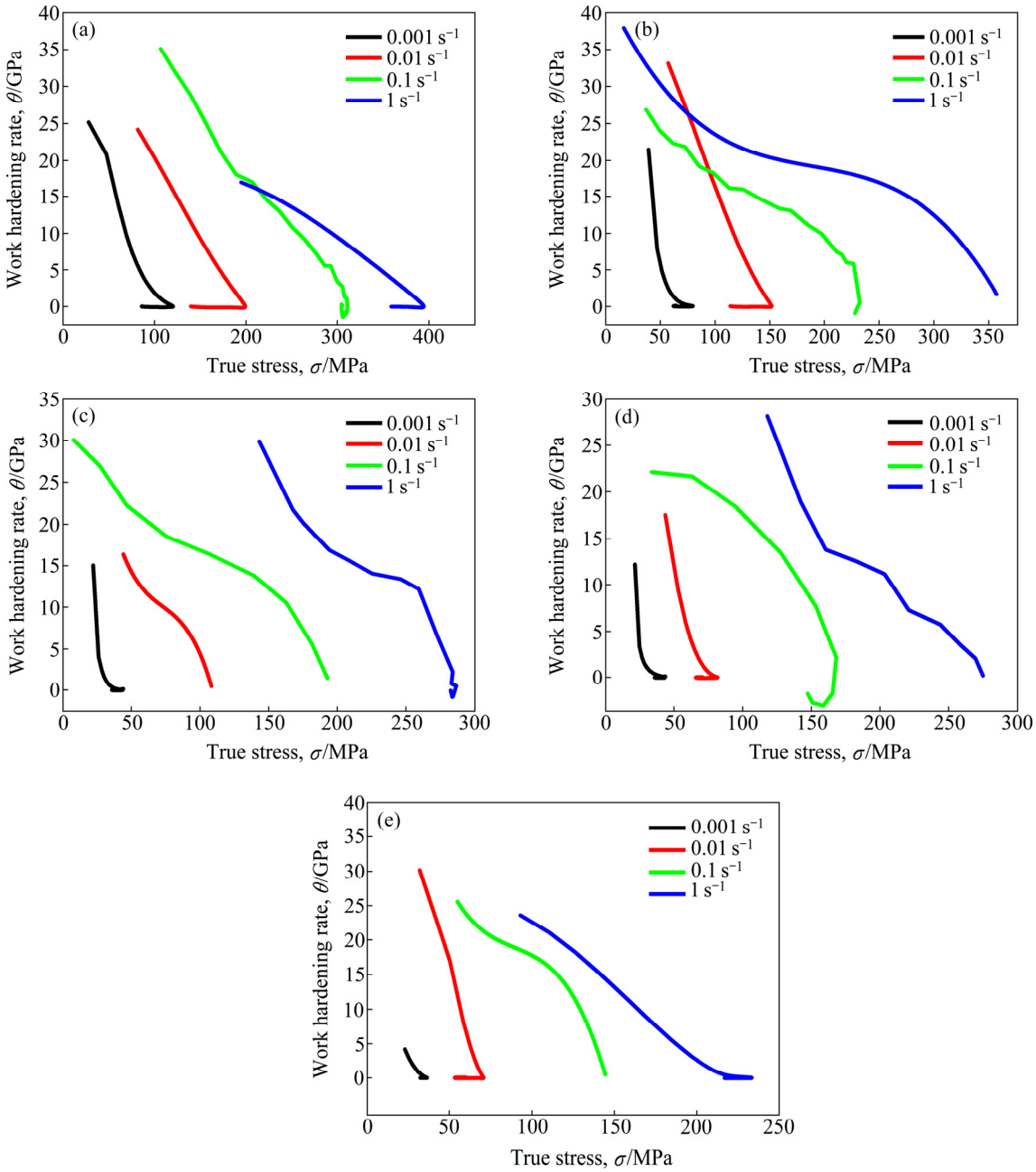

Fig. 7 Work hardening curves of Ti−3.5Al−5Mo−6V−3Cr−2Sn−0.5Fe−0.1B−0.1C alloy: (a) 750 °C; (b) 790 °C; (c) 830 °C; (d) 870 °C; (e) 910 °C

This is because the reduction of the strain rate provides sufficient movement time for the dislocation, reducing the critical shear stress required for the deformation of the slip system and the work hardening effect.

According to Figs. 3 and 4, it is known that the main softening mechanism occurring during the thermal deformation of the alloy is DRX. POLIAK and JONAS [31] studied the critical conditions of DRX. It is found that whether the alloy undergoes DRX is determined by the stored distortion energy during the deformation process. When the distortion energy is large enough, DRX will occur, and this critical point corresponds to the position of $-(\partial\theta/\partial\sigma)$=Minimum or $-(\partial\ln\theta/\partial\varepsilon)$=Minimum on the work hardening curves, as pointed out by black arrows in Figs. 8(a−e).

The critical stress at the beginning of DRX is shown in Fig. 8(f). It can be found that DRX prefers to happen at a higher temperature and a lower strain rate, which is consistent with the analysis of microstructure evolution shown in Figs. 3 and 4 that DRX prefers to happen at high temperatures and low strain rates.

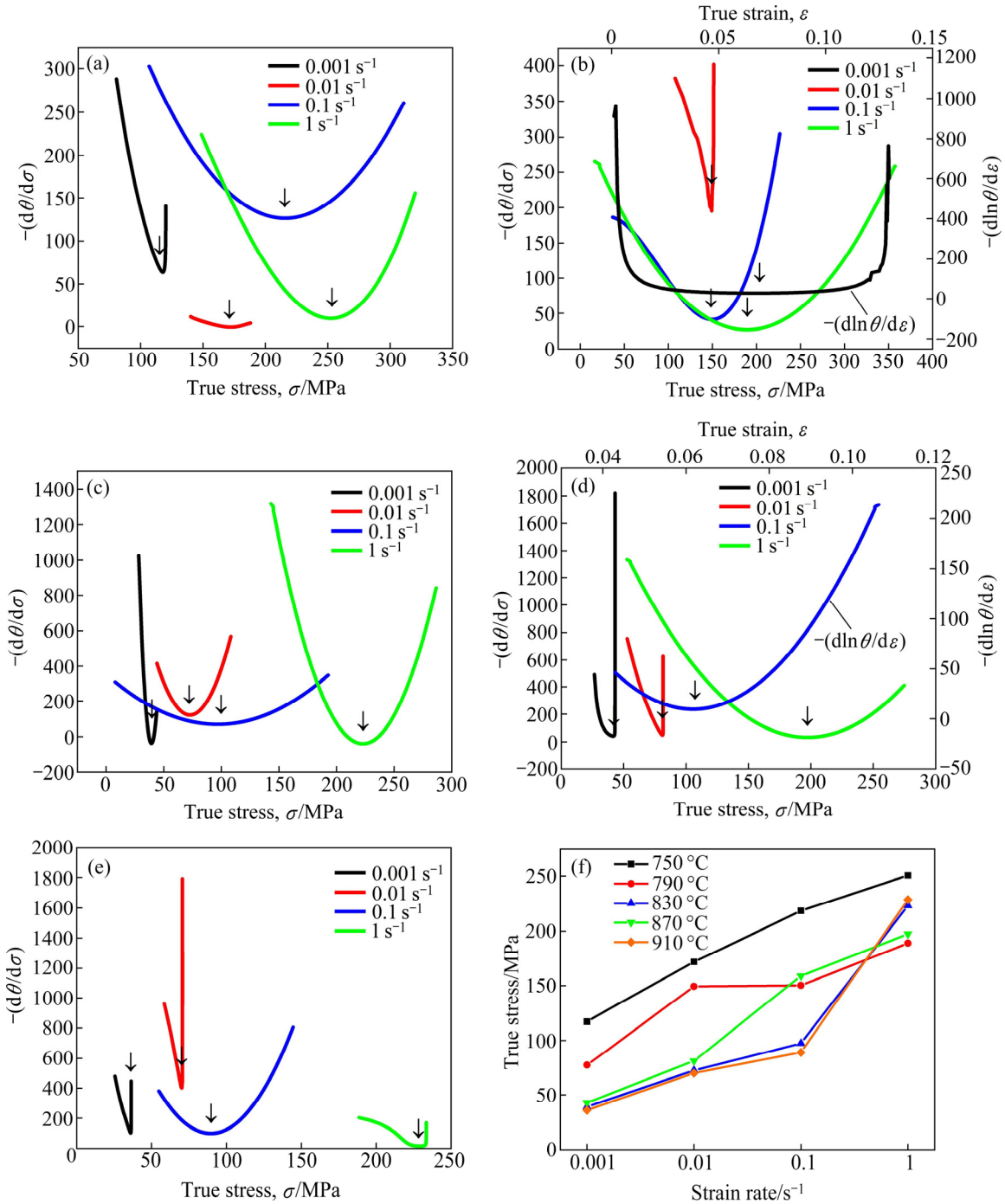

Fig. 8 Flow stress dependence of −(dθ/dσ) or −(dln θ/dε) for alloy deformed in different conditions (a−e) and critical stress at beginning of DRX (f): (a) 750 °C; (b) 790 °C; (c) 830 °C; (d) 870 °C; (e) 910 °C

In some results of the present work, the change of work hardening rate θ is relatively gentle, and the position of the critical point is not obvious, which may be related to slow diffusion elements such as Mo and V with relatively high alloying content [32]. The addition of these elements slows down the diffusion of atoms and the migration of grain boundaries, while DRX is essentially the movement of dislocations and the migration of grain boundaries. It makes the DRX process proceed smoothly, and the inflection point on the work hardening curve becomes covert.

3.4 Constitutive model

Arrhenius model [33] is an effective method used in recent years to study the relationship between the flow behavior and deformation parameters. The formula is as follows:

$$\dot{\varepsilon} = AF(\sigma)\exp[-Q/(RT)] \tag{1}$$

$$F(\sigma)=\begin{cases}\sigma^{n_1}, & \alpha\sigma<0.8\\ \exp(\beta\sigma), & \alpha\sigma<1.2\\ [\sinh(\alpha\sigma)]^n, & \text{for all stress levels}\end{cases} \tag{2}$$

where $\dot{\varepsilon}$ is the strain rate (s^{-1}), σ is the flow stress (MPa), R is the gas constant (8.314 J/(mol·K)), T is the deformation temperature (K), and A, β, α, and n are the material constants. These constants can be obtained by the following formula:

$$\alpha=\beta/n_1 \tag{3}$$

$$\ln\dot{\varepsilon} = \ln A + n_1\ln\sigma - Q/(RT) \tag{4}$$

$$\ln\dot{\varepsilon} = \ln A + \beta\sigma - Q/(RT) \tag{5}$$

$$\ln\dot{\varepsilon} = \ln A + n\ln[\sinh(\alpha\sigma)] - Q/(RT) \tag{6}$$

To solve the relevant parameters, the derivatives of the two ends of Eqs. (4)−(10) are taken:

$$n_1 = \left(\frac{\partial\ln\dot{\varepsilon}}{\partial\ln\sigma}\right)_T \tag{7}$$

$$\beta = \left(\frac{\partial\ln\dot{\varepsilon}}{\partial\sigma}\right)_T \tag{8}$$

$$n = \left[\frac{\partial\ln\dot{\varepsilon}}{\partial\ln\sinh(\alpha\sigma)}\right]_T \tag{9}$$

$$Q = nR\left[\frac{\partial\ln\sinh(\alpha\sigma)}{\partial(1/T)}\right]_T \tag{10}$$

According to Eqs. (7)−(10), it can be found that the solution of these parameters needs to be fitted to $\ln\sigma$−$\ln\dot{\varepsilon}$, σ−$\ln\dot{\varepsilon}$, $\ln[\sinh(\alpha\sigma)]$−$\ln\dot{\varepsilon}$, and $\ln[\sinh(\alpha\sigma)]$−$1/T$, respectively, as shown in Fig. 9. In the present work, the peak stress is chosen as representative value to further describe the derivation process. Parameters obtained under different conditions are averaged as the final value. The final results of each parameter are listed in Table 1.

Zeller−Hollomon [34] links the flow behaviors to the activation energy during hot deformation and proposes the parameter Z. Thus, the constitutive equation can be expressed as

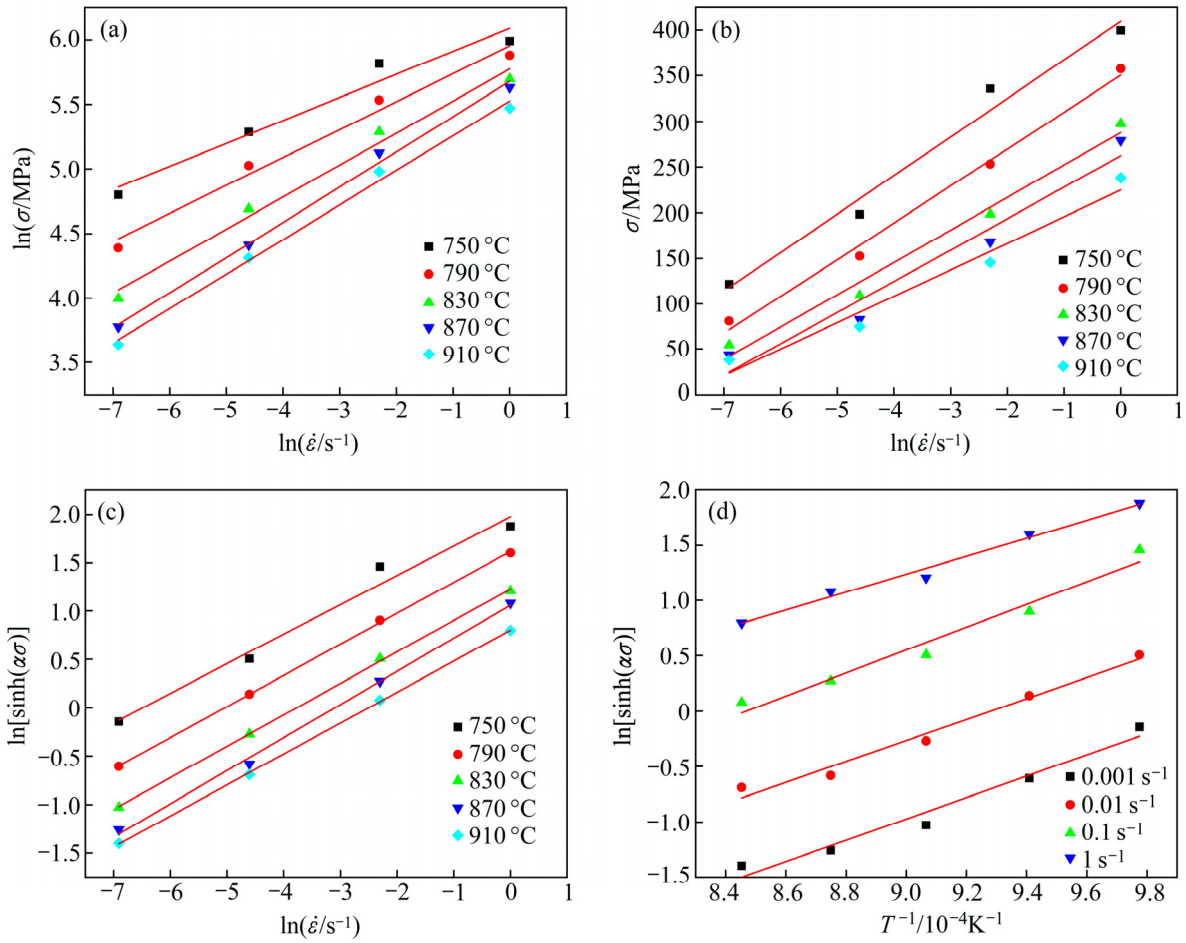

Fig. 9 Fitting curves required to solve constitutive equation: (a) $\ln\sigma$−$\ln\dot{\varepsilon}$; (b) σ−$\ln\dot{\varepsilon}$; (c) $\ln[\sinh(\alpha\sigma)]$−$\ln\dot{\varepsilon}$; (d) $\ln[\sinh(\alpha\sigma)]$−$1/T$

Table 1 Results of material parameters

n_1	β	α	n	Q/(kJ·mol^{-1})	A
4.3367	0.02799	0.006454	3.107	242.78	$e^{22.406}$

$$Z=\dot{\varepsilon}\exp[-Q/(RT)]=A[A\sinh(\alpha\sigma)]^n \tag{11}$$

$$\sigma=\frac{1}{\alpha}\ln\left\{(Z/A)^{\frac{1}{n}}+\left[(Z/A)^{\frac{2}{n}}+1\right]^{\frac{1}{2}}\right\} \tag{12}$$

Finally, the constitutive equation of the Ti−3.5Al−5Mo−6V−3Cr−2Sn−0.5Fe−0.1B−0.1C alloy is as follows:

$$\dot{\varepsilon}=e^{22.406}[\sinh(0.006454\sigma)]^{3.107}\cdot \exp[-242783.5/(RT)] \tag{13}$$

$$\sigma=154.943\ln\left\{\left(\frac{Z}{e^{22.406}}\right)^{\frac{1}{3.107}}+\left[\left(\frac{Z}{e^{22.406}}\right)^{\frac{2}{3.107}}+1\right]^{\frac{1}{2}}\right\} \tag{14}$$

where $Z=\dot{\varepsilon}\exp[242783.5/(RT)]$.

To verify the accuracy of the obtained constitutive equation, the theoretical peak stress of the alloy is solved using Eqs. (13) and (14). And compared with the experimental values, the relative average error of the constitutive equation is about 4.98%, which indicates that the equation is reasonably accurate. DRV is completed by the migration of dislocations and its activation energy is similar with the self-diffusion energy [35]. The occurrence of DRX is more dependent on the movement of grain boundaries, which requires higher activation energy. In the present work, the activation energy of the Ti−3.5Al−5Mo−6V−3Cr−2Sn−0.5Fe−0.1B−0.1C alloy is 242.78 kJ/mol, which is significantly higher than the self-diffusion energy of pure β titanium alloy (153 kJ/mol). This indicates that the main mechanism of the alloy during hot deformation is DRX, which is consistent with the analysis results of the microstructure evolution.

3.5 Processing map

Processing map is widely used to study the hot deformation behavior and provides design guidance for hot working processes. The most common one is the processing map based on the dynamic materials model (DMM). In the DMM model, the total energy in the deformation process is dissipated mainly through two aspects:

$$P=\sigma\cdot\dot{\varepsilon}=G+J=\int_0^{\dot{\varepsilon}}\sigma\mathrm{d}\dot{\varepsilon}+\int_0^{\sigma}\dot{\varepsilon}\mathrm{d}\sigma \tag{15}$$

where G represents the energy consumed during the plastic deformation of the alloy, and J represents the energy required for the evolution of the alloy during plastic deformation. The relative magnitude of these two parts of energy is determined by the strain rate sensitivity coefficient m during deformation, and m can be calculated by the stress and strain:

$$\frac{\mathrm{d}J}{\mathrm{d}G}=\frac{\dot{\varepsilon}\mathrm{d}\sigma}{\sigma\mathrm{d}\dot{\varepsilon}}=\frac{\mathrm{d}(\ln\sigma)}{\mathrm{d}(\ln\dot{\varepsilon})}\approx\frac{\Delta\log\sigma}{\Delta\log\dot{\varepsilon}}=m \tag{16}$$

$$\sigma=K\dot{\varepsilon}^m \tag{17}$$

$$m=\frac{\partial\ln\sigma}{\partial\ln\dot{\varepsilon}} \tag{18}$$

where K represents the flow stress when the strain rate is 1 s^{-1}. When m=1, the alloy is in an ideal linear dissipation state.

To quantitatively analyze the energy dissipation, the power dissipation efficiency η is introduced. This parameter characterizes the proportional relationship between J and G during alloy deformation:

$$\eta=\frac{J}{J_{\max}}=\frac{2m}{m+1} \tag{19}$$

Combining parameters of T, $\dot{\varepsilon}$ and η can get the power dissipation map of hot deformation. The higher the value of η is, the more the energy is consumed by the evolution of the structure during the deformation of the alloy, and the hot deformation of the alloy is more stable at this time. Based on this theory, in the hot deformation process of titanium alloy, the region where η is greater than 35% is usually regarded as the stable region [10,36,37]. However, there are many deformation mechanisms in the thermal processing process, such as DRV, DRX, and the formation of holes. Each deformation mechanism has its corresponding η, so the area with a small η cannot be simply regarded as an unstable area.

In this case, many researchers have put forward their instability criterion, of which the Prasad criterion is the most widely used:

$$\xi_{\mathrm{p}}(\dot{\varepsilon},T)=\frac{\partial\ln[m/(m+1)]}{\partial\ln\dot{\varepsilon}}+m<0 \tag{20}$$

When the parameter ξ_P is less than 0, the deformation of the alloy will be in an unstable state. The processing map of the alloy is obtained by combining the power dissipation map and the instability map. Figure 10 shows the processing maps of Ti−3.5Al−5Mo−6V−3Cr−2Sn−0.5Fe−0.1B−0.1C alloy at different strains (ε=0.2, 0.4, 0.6).

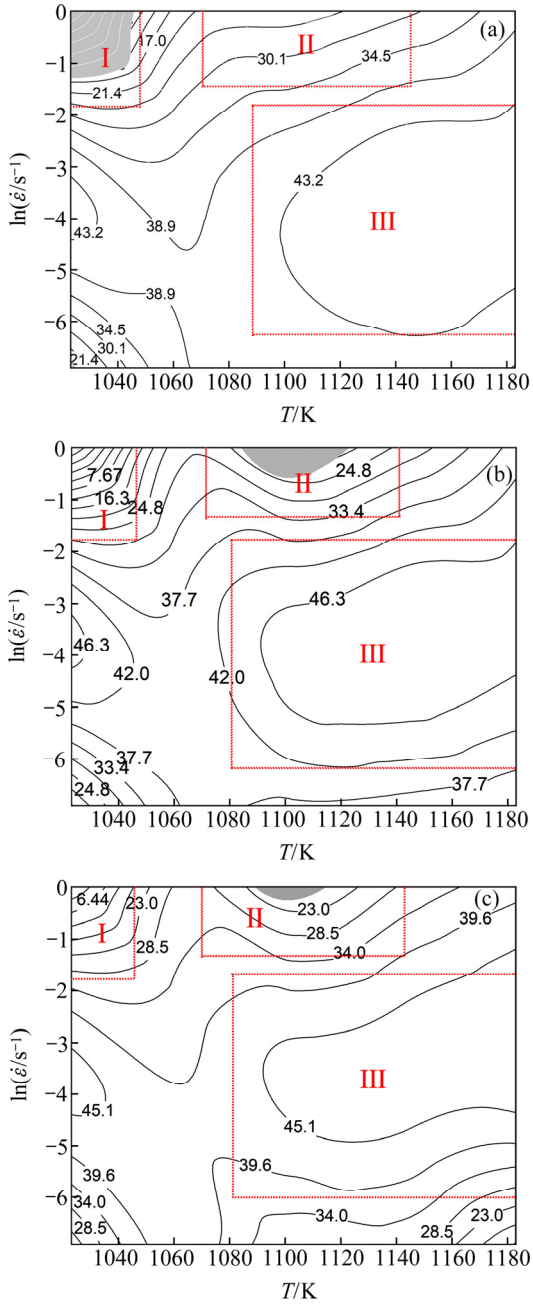

Fig. 10 Processing maps of Ti−3.5Al−5Mo−6V−3Cr−2Sn−0.5Fe−0.1B−0.1C alloy with different strain: (a) ε=0.2; (b) ε=0.4; (c) ε=0.6

According to the energy dissipation and stability of the alloy during deformation, the processing map can be divided into three regions (Regions I, II, III). When the strain is 0.2, it can be found from Fig. 10(a) that the instability region (gray region) of the alloy shows up in Region I. In Region I, the power dissipation efficiency η is significantly lower than the critical stability value of 35%. This shows that when the alloy undergoes thermal deformation under this condition (low temperature and high strain rates), the main deformation mechanism may be cracking and adiabatic shearing, which exhibit unstable characteristics [21,38]. In Region II, η increases to about 30%, which is higher than the value in Region I but still lower than the critical value. However, there is no unstable region, which indicates that besides stable mechanisms such as DRV and DRX, the deformation process under this condition may also be accompanied by a few unstable mechanisms. In Region III, the value of η reaches its maximum of about 43%. When the alloy deforms under the condition of this region, DRV and DRX should be the main mechanisms, which can be proven by the results of microstructures shown in Fig. 3.

When the strain increases to 0.4, the unstable region disappears in Region I. But the value of η is still very low, less than 20%. Although there is no unstable region, the deformation of the alloy at this time is still dominated by some unstable mechanisms. Therefore, this area should be avoided during thermal processing. In Region II, the unstable region appears in the condition of 1085−1120 K and 0.1−1 s^{-1}. And the maximum value of η still appears in Region III. With further increasing the strain to 0.6, the overall structure of the processing map has no significant change compared with that at the strain of 0.4. The unstable region still appears in Region II, and Region III is still the most stable region of deformation with the highest power dissipation efficiency. This indicates that as the strain increases, the unstable region of deformation gradually changes toward high temperature and high strain rate. Moreover, the unstable area of the alloy gradually shrinks, indicating that the alloy studied in the present work has excellent hot workability.

3.6 Analysis of abnormal flow behavior

Through the obtained compression curves shown in Fig. 1, we can divide the curves into two types according to different shapes. The first is the

typical flow curves (when $\dot{\varepsilon}$=0.001, 0.01 and 1 s^{-1}), which show common features of work-hardening effect and dynamic softening behavior, including DRX and DRV. The other is the curves at the strain rate of 0.1 s^{-1}, as shown in Fig. 1(c) which include two different peak stresses.

Similar flow curves also showed up in other works. GUO et al [39] conducted the same compression tests on MoNbHfZrTi high entropy alloy. The experimental results at 900 °C and $\dot{\varepsilon}$= 0.1 s^{-1} also showed a strange shape that as the strain increased, the stress first reached a peak and then decreased to a certain value. As the deformation continued, the stress started to increase to another peak again and then decreased gradually until a steady state. This was attributed to the alternation of dislocation proliferation and DRV mechanism in the deformation process. However, there is only an assumption and the specific reason is not analyzed yet. To better analyze the abnormal flow behavior shown in the present research, the compression curves are divided into three parts, as shown in Fig. 11. The first part is a normal increase of stress to the first peak σ_{p1} followed by a subsequent drop. It can be regarded as a kind of special yield phenomenon called discontinuous yielding phenomenon (DYP), which can be attributed to the dislocation proliferation and activation of slipping systems during the deformation process [40].

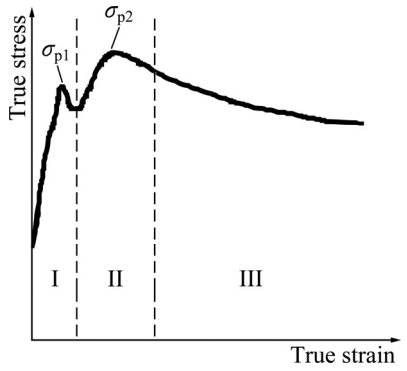

Fig. 11 Abnormal flow curve at strain rate of 0.1 s^{-1}

The second part contains second peak, which is the key content to be analyzed. Figure 12 shows the misorientation analysis result after hot compression at 910 °C and different strain rates, in which point-to-point misorientation and point-to-origin misorientation are represented by red and blue lines, respectively. It can be found that the misorientation curves under three deformation parameters show a similar trend that the point-to-origin misorientations are high while the point-to-point misorientations keep a relatively low value. This means that the misorientation inside grains is a cumulative process, consistent with the continuous dynamic recrystallization (CDRX) mechanism that attributes the formation of recrystallized grains to the formation and rotation of subgrains. For CDRX, DRX grains prefer to nucleate along original boundaries and locations of the triple junctions with similar orientations. At this time, newly-formed grains only have a limited hindrance effect to dislocation movement. During the deformation process, the formed grains begin to absorb dislocations and rotate to the preferred slip systems, which results in anisotropic orientations and strong barrier to dislocation mobility [41]. This makes the stress start to increase again and reach the second peak σ_{p2}. And as deformation continues, a large number of DRX grains complete the rotation and their hindrance effect becomes weak. Dynamic softening mechanism becomes the essential effect again, which results in the decrease of stress as strain increases.

To better understand the abnormal flow behavior, additional EBSD analysis was performed and the results are shown in Fig. 13. According to KAM maps, as the strain rate increases, it can be distinctly identified that dislocation density increases rapidly (represented by green color), which is in line with our previous analysis. In addition, the local misorientation distribution, as shown in Fig. 13, also illustrates that the value above 0.4° increases firstly with a following decrease as strain rates increase and reaches a maximum value of 9.36 at the strain rate of 0.1 s^{-1}. Above results show that the recrystallized grains achieve the maximum rotation at the strain rate of 0.1 s^{-1} although the dislocation density is lower than that at 1 s^{-1}, which can severely hinder dislocation movement and result in the abnormal flow behavior shown in Fig. 11.

From Fig. 1, we can find that such an abnormal flow behavior only occurs at the strain rate of 0.1 s^{-1}. It can be explained through the following reasons. When the strain rate is relatively low, the density of dislocation is low and the degree of deformation is not enough to trigger rotation of DRX grains, which indicates the hardening effect caused by DRX grain is too weak compared to the dynamic softening mechanism and there is no

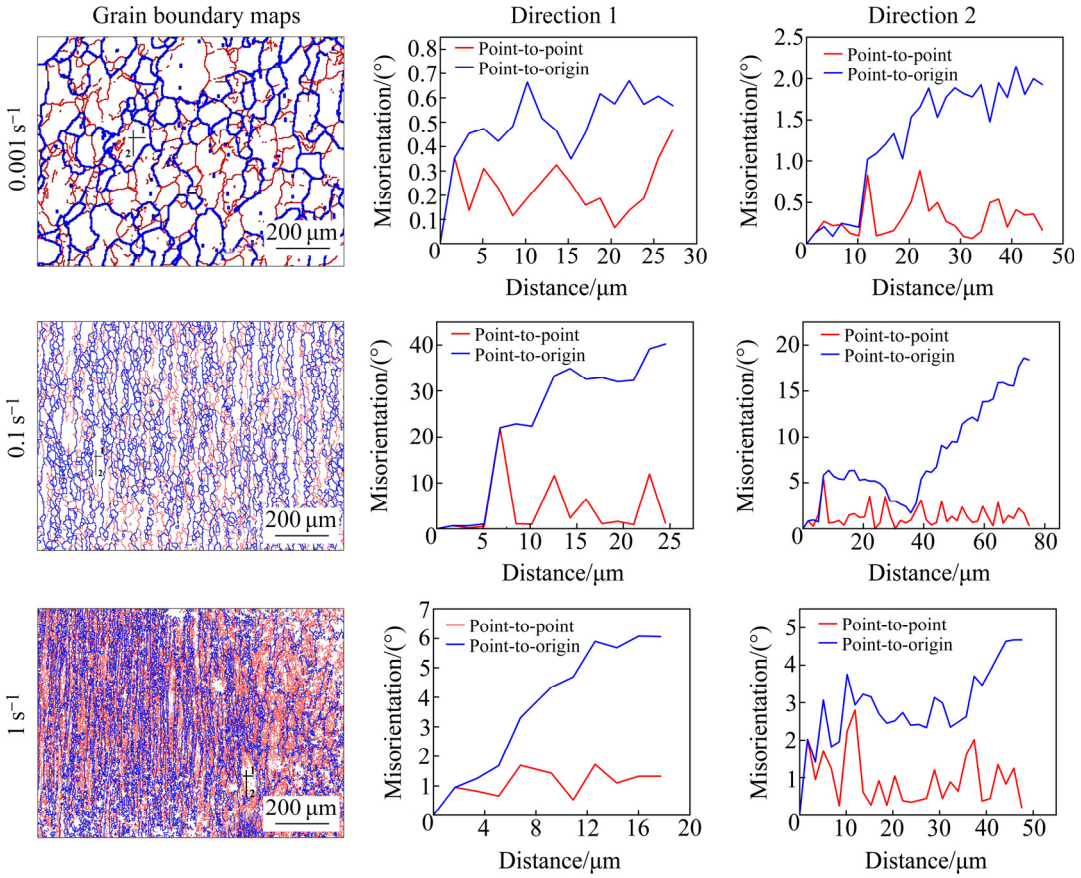

Fig. 12 Misorientations along horizontal (Direction 1) and vertical (Direction 2) lines deformed at different strain rates and fixed temperature of 910 °C

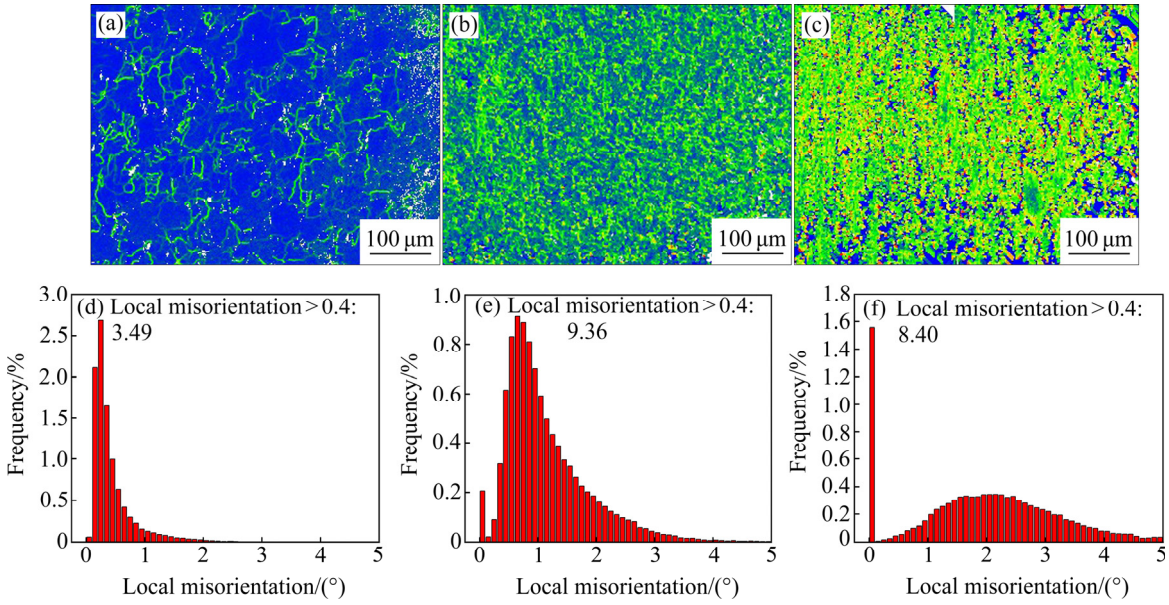

Fig. 13 EBSD result of KAM maps (a−c) and local misorientation distribution (d−f) of alloy deformed at 910 °C and different strain rates: (a, d) 0.001 s^{-1}; (b, e) 0.1 s^{-1}; (c, f) 1 s^{-1}

obvious influence on flow behavior. When the strain rate reaches 1 s^{-1}, there is not sufficient time for dislocation motion, which can significantly influence the formation of DRX grains. It can also be verified by Fig. 4 that while the strain rate is high, it is difficult to distinguish the occurrence of DRX grains. Therefore, for both relatively high and low strain rates, the hardening effect resulting from

rotation of DRX grains can be negligible compared with the softening effect.

4 Conclusions

(1) The stress−strain curves show the typical features of the work-hardening effect and the dynamic softening mechanism: as the strain increases, stress first increases to reach a peak and then decreases gradually. The occurrence of DRX can be verified by the microstructure observation when the temperature reaches 790 °C.

(2) The work-hardening curves are calculated and the critical stress is located at the lowest point. As the strain increases or the strain rate decreases, the work-hardening rate (θ) decreases gradually, which reflects the dynamic softening mechanism. And as the strain rate increases or the temperature decreases, the critical stress of DRX increases gradually, which indicates that DRX prefers to happen at relatively high temperatures and low strain rates.

(3) Constitutive equation of Ti−3.5Al−5Mo−6V−3Cr−2Sn−0.5Fe−0.1B−0.1C alloy is $\dot{\varepsilon} = e^{22.406} \times [\sinh(0.006454\sigma)^{3.107}]\exp[-242783.5/(RT)]$. The deformation activation energy is 242.78 kJ/mol, which is higher than the self-diffusion energy of pure β titanium alloy and indicates the occurrence of DRX.

(4) The processing maps at different strains (ε=0.2, 0.4, 0.6) are obtained by the dynamic materials model and the Prasad criterion. It is found that the Ti−3.5Al−5Mo−6V−3Cr−2Sn−0.5Fe−0.1B−0.1C alloy has a wide hot processing window, which represents its excellent hot workability.

(5) When the strain rate is 0.1 s^{-1}, the stress−strain curves exhibit an abnormal shape, that is, the stress can reach two different peaks during deformation. Through EBSD measurement, the main DRX mechanism is determined to be continuous dynamic recrystallization (CDRX) and the strange flow behavior can be attributed to the alternation of hardening effect caused by the rotation of DRX grains and dynamic softening mechanism.

References

[1] BOYER R R, BRIGGS R D. The use of β titanium alloys in the aerospace industry [J]. Journal of Materials Engineering and Performance, 2013, 22: 2916−2920. https://doi.org/10.1007/s11665-013-0728-3.

[2] HUANGC W, ZHAOY Q, XINS W, TAN C S, ZHOU W, LI Q, ZENG W D. Effect of microstructure on high cycle fatigue behavior of Ti−5Al−5Mo−5V−3Cr−1Zr titanium alloy [J]. International Journal of Fatigue, 2017, 94: 30−40. https://doi.org/10.1016/j.ijfatigue.2016.09.005.

[3] WAN M P, ZHAO Y Q, ZENG W D, CAI G. Effects of cold pre-deformation on aging behavior and mechanical properties of Ti-1300 alloy [J]. Journal of Alloys and Compounds, 2015, 619: 383−388. https://doi.org/10.1016/j.jallcom.2014.09.064.

[4] GAO P F, ZHAN M, FAN X G, LEI Z N, CAI Y. Hot deformation behavior and microstructure evolution of TA15 titanium alloy with nonuniform microstructure [J]. Materials Science & Engineering A, 2017, 689: 243−251. https://doi.org/10.1016/j.msea.2017.02.054.

[5] SUJOY K K, ATASI G, NISHANT F, AMIT B. Quantitative microstructural characterization of a near beta Ti alloy, Ti-5553 under different processing conditions [J]. Materials Characterization, 2013, 81: 37−48. https://doi.org/10.1016/j.matchar.2013.03.016.

[6] WU C, HUANG L, LI C M. Experimental investigation on dynamic phase transformation and texture evolution of Ti55531 high strength titanium alloy during hot compression in the α+β region [J]. Materials Science and Engineering A, 2020, 773: 138851. https://doi.org/10.1016/j.msea.2019.138851.

[7] YANG H, GAO P F, FAN X G, LI H W, SUN Z C, LI H, GUO L G, ZHAN M, LIU Y L. Some advances in plastic forming technologies of titanium alloys [J]. Procedia Engineering, 2014, 81: 44−53. https://doi.org/10.1016/j.proeng.2014.09.127.

[8] GUO L G, FAN X G, YU G F, YANG H. Microstructure control techniques in primary hot working of titanium alloy bars: A review [J]. Chinese Journal of Aeronautics, 2016, 29: 30−40. https://doi.org/10.1016/j.cja.2015.07.011.

[9] GAO P F, FU M W, ZHAN M, LEI Z N, LI Y X. Deformation behavior and microstructure evolution of titanium alloys with lamellar microstructure in hot working process: A review [J]. Journal of Materials Science & Technology, 2020, 39: 56−73. https://doi.org/10.1016/j.jmst.2019.07.052.

[10] ZHAO Q Y, YANG F, TORRENS R, BOLZONI L. Comparison of hot deformation behaviour and microstructural evolution for Ti−5Al−5V−5Mo−3Cr alloys prepared by powder metallurgy and ingot metallurgy approaches [J]. Materials & Design, 2019, 169: 107682. https://doi.org/10.1016/j.matdes.2019.107682.

[11] MARYAM M, ALIREZA H. Hot working behavior of near alpha titanium alloy analyzed by mechanical testing and processing map [J]. Transactions of Nonferrous Metals Society of China, 2020, 30: 1560−1573. https://doi.org/10.1016/S1003-6326(20)65319-5.

[12] XIA Y F, JIANG W, CHENG Q, JIANG L, JIN L. Hot deformation behavior of Ti−6Al−4V−0.1Ru alloy during isothermal compression [J]. Transactions of Nonferrous

Metals Society of China, 2020, 30: 134−146. https://doi.org/10.1016/S1003-6326(19)65186-1.

[13] RAVINDRANADH B, VEMURI M. Constitutive modeling of dynamic flow behavior of Ti-5553 alloy [J]. Journal of Alloys and Compounds, 2019, 787: 260−266. https://doi.org/10.1016/j.jallcom.2019.02.101.

[14] WANG Z, WANG X N, ZHU Z S. Characterization of high-temperature deformation behavior and processing map of TB17 titanium alloy [J]. Journal of Alloys and Compounds, 2017, 692: 149−154. https://doi.org/10.1016/j.jallcom.2016.09.012.

[15] ZHANG C J, KONG F T, XIAO S L, ZHAO E T, XU L J, CHEN Y Y. Evolution of microstructure and tensile properties of in situ titanium matrix composites with volume fraction of (TiB+TiC) reinforcements [J]. Materials Science & Engineering A, 2012, 548: 152−160. https://doi.org/10.1016/j.msea.2012.04.004.

[16] HUANG L J, GENGL, PENGH X. In situ (TiB_w+TiC_p)/Ti6Al4V composites with a network reinforcement distribution [J]. Materials Science & Engineering A, 2010, 527: 6723−6727. https://doi.org/10.1016/j.msea.2010.07.025.

[17] CHEN Y Y, DUZ X, XIAO S L, XU L J, TIAN J. Effect of aging heat treatment on microstructure and tensile properties of a new β high strength titanium alloy [J]. Journal of Alloys and Compounds, 2014, 586: 588−592. https://doi.org/10.1016/j.jallcom.2013.10.096.

[18] TAKU S, ANDREY B, RUSTAM K, HIROMI M, JOHN J J. Dynamic and post-dynamic recrystallization under hot, cold and severe plastic deformation conditions [J]. Progress in Materials Science, 2014, 60: 130−207. https://doi.org/10.1016/j.pmatsci.2013.09.002.

[19] SEMIATINS L, SEETHARAMANV, WEISS I. Flow behavior and globularization kinetics during hot working of Ti−6Al−4V with a colony alpha microstructure [J]. Materials Science & Engineering A, 1999, 263: 257−271. https://doi.org/10.1016/S0921-5093(98)01156-3.

[20] ZHANG S L, SUN X J, DONG H. Effect of deformation on the evolution of spheroidization for the ultra high carbon steel [J]. Materials Science & Engineering A, 2006, 432: 324−332. https://doi.org/10.1016/j.msea.2006.06.057.

[21] SEMIATINS L, BIELERT R. The effect of alpha platelet thickness on plastic flow during hot working of Ti−6Al−4V with a transformed microstructure [J]. Acta Materialia, 2011, 49: 3565−3573. https://doi.org/10.1016/S1359-6454(01)00236-1.

[22] WANG M, HUANG M X. Abnormal TRIP effect on the work hardening behavior of a quenching and partitioning steel at high strain rate [J]. Acta Materialia, 2020, 188: 551−559. https://doi.org/10.1016/j.actamat.2020.02.035.

[23] YANG J L, WANG G F, JIAO X Y, LI Y, LIU Q. High-temperature deformation behavior of the extruded Ti−22Al−25Nb alloy fabricated by powder metallurgy [J]. Materials Characterization, 2018, 137: 170−179. https://doi.org/10.1016/j.matchar.2018.01.019.

[24] CHEN F, CUIZ S, CHENS J. Recrystallization of 30Cr2Ni4MoV ultra-super-critical rotor steel during hot deformation. Part I: Dynamic recrystallization [J]. Materials Science & Engineering A, 2011, 528: 5073−5080. https://doi.org/10.1016/j.msea.2011.03.008.

[25] VICTOR C O, CAMILO A F S, KAIO N C. α phase precipitation and mechanical properties of Nb-modified Ti-5553 alloy [J]. Materials Science & Engineering A, 2016, 670: 112−121. https://doi.org/10.1016/j.msea.2016.06.001.

[26] WANG Y T, LI J B, XIN Y C, CHEN X H, RASHAD M, LIU B, LIU Y. Hot deformation behavior and hardness of a CoCrFeMnNi high-entropy alloy with high content of carbon [J]. Acta Metallurgica Sinica (English Letters), 2019, 32: 932−943. https://doi.org/10.1007/s40195-019-00916-0.

[27] ZHANG J Y, JIANG P, ZHU Z L, CHEN Q, ZHOU J, MENG Y. Tensile properties and strain hardening mechanism of Cr−Mn−Si−Ni alloyed ultra-strength steel at different temperatures and strain rates [J]. Journal of Alloys and Compounds, 2020, 842: 155856. https://doi.org/10.1016/j.jallcom.2020.155856.

[28] REID C N, OWEN W S. Deformation geometry for materials scientists [M]. Elsevier, 1973. https://doi.org/10.1107/S0021889876010583.

[29] MURUGESAN A, NIMA H, ADAM T,PETER H, DANIEL F. Dynamic recrystallization behaviour of $Al_xCoCrFeNi$ high entropy alloys during high-temperature plane strain compression [J]. Materials Science & Engineering A, 2019, 745: 90−106. https://doi.org/10.1016/j.msea.2018.12.102.

[30] MCQUEEN H J, YUE S, RYAN N D. Hot-working characteristics of steels in austenitic state [J]. Journal of Materials Processing Technology, 1995, 53: 293−310. https://doi.org/10.1016/0924-0136(95)01987-P.

[31] POLIAK E I, JONAS J J. A one-parameter approach to determining the critical conditions for the initiation of dynamic recrystallization [J]. Acta Materialia, 1996, 44: 127−136. https://doi.org/10.1016/1359-6454(95)00146-7.

[32] JAMES D C, ROBERT D B, RODNEY R B, SESH T, PATRICK R, NIKOLAY S, JOHN C F. State of the art in Beta titanium alloys for airframe applications [J]. JOM, 2015, 67: 1281−1303. https://doi.org/10.1007/s11837-015-1442-4.

[33] SELLARS C M, TEGART W J. Hot workability [J]. International Materials Reviews, 1972, 17: 1−24. https://doi.org/10.1179/imtlr.1972.17.1.1.

[34] ZENER C, HOLLOMON J H. Effect of strain rate upon plastic flow of steel [J]. Journal of Applied Physics, 1944, 15: 22−32. https://doi.org/10.1063/1.1707363.

[35] JONES N G, DASHWOOD R J, DYE D, JACKSON M. Thermomechanical processing of Ti−5Al−5Mo−5V−3Cr [J]. Materials Science & Engineering A, 2008, 490: 369−377. https://doi.org/10.1016/j.msea.2008.01.055.

[36] PRASAD Y V R K, SESHACHARYULU T. Processing maps for hot working of titanium alloys [J]. Materials Science & Engineering A, 1998, 243: 82−88. https://doi.org/10.1016/S0921-5093(97)00782-X.

[37] HIROAKI M, KITAMURA M, LI Y P, KOIZUMI Y, CHIBA A. Hot forging characteristic of Ti−5Al−5V−5Mo−3Cr alloy with single metastable β microstructure [J]. Materials Science & Engineering A, 2014, 611: 337−344. https://doi.org/10.1016/j.msea.2014.06.006.

[38] ZHENG Y P, ZENG W D, WANG Y B, ZHOU D D, GAO X X. High strain rate compression behavior of a heavily stabilized beta titanium alloy: Kink deformation and adiabatic shearing [J]. Journal of Alloys and Compounds, 2017, 708: 84−92. https://doi.org/10.1016/j.jallcom.2017.02.

284.
[39] GUO N N, WANG L, LUOL S, LI X Z, CHEN R R, SU Y Q, GUO J J, FU H Z. Hot deformation characteristics and dynamic recrystallization of the MoNbHfZrTi refractory high-entropy alloy [J]. Materials Science & Engineering A, 2016, 651: 698−707. https://doi.org/10.1016/j.msea.2015.10.113.
[40] PHILIPPART I, RACKH J. High temperature dynamic yielding in metastable Ti−6.8Mo−4.5F−1.5Al [J]. Materials Science & Engineering A, 1998, 243: 196−200. https://doi.org/10.1016/S0921-5093(97)00800-9.
[41] CHEN Y, LI J S, TANG B, KOU H C, ZHANG F S, CHANG H, ZHOU L. Grain boundary character distribution and texture evolution in cold-drawn Ti−45Nb wires [J]. Materials Letters, 2013, 98: 254−257. https://doi.org/10.1016/j.matlet.2013.02.043.

一种新型亚稳 β 钛合的热变形行为及显微组织演变表征

陈兆琦[1,2]，徐丽娟[1,2]，曹守臻[3]，杨建凯[1,2]，郑云飞[1,2]，肖树龙[1,2]，田竟[1,2]，陈玉勇[1,2]

1. 哈尔滨工业大学 金属精密热加工国家重点实验室，哈尔滨 150001；
2. 哈尔滨工业大学 材料科学与工程学院，哈尔滨 150001；
3. 黄山学院 机电工程学院，黄山 245021

摘 要：通过热压缩实验研究 Ti−3.5Al−5Mo−6V−3Cr−2Sn−0.5Fe−0.1B−0.1C 锻态合金在 750～900 ℃温度范围和 0.001～1 s^{-1} 应变速率范围内的热变形特征。应力−应变曲线表明，流变应力随着温度的提高和应变速率的降低而降低。显微组织对热变形参数十分敏感，当应变速率保持在 0.001 s^{-1} 不变，温度达到 790 ℃或者温度保持在 910 ℃不变，应变速率不高于 0.1 s^{-1} 时合金显微组织中出现动态再结晶晶粒。计算出加工硬化率 θ，并发现动态再结晶倾向于在较高温度和较低应变速率条件下发生。得到合金的本构方程和加工硬化图，平均热激活能为 242.78 kJ/mol，而且只有少量失稳区在热加工图中出现，说明合金具有良好的热加工性能。当应变速率为 0.1 s^{-1} 时，应力−应变曲线呈现一种异常的形状，连续出现两个应力峰值，这一现象可以归因于连续动态再结晶和再结晶晶粒的转动所造成的硬化现象与动态软化机制的混合作用。

关键词：亚稳 β 钛合金；热变形行为；显微组织演变；异常流变行为

(Edited by Bing YANG)